IEEE Access
Multidisciplinary | Rapid Review | Open Access Journal

Received 5 May 2024, accepted 20 May 2024, date of publication 22 May 2024, date of current version 30 May 2024.

*Digital Object Identifier 10.1109/ACCESS.2024.3404269*

RESEARCH ARTICLE

# Assessment of Unknown Parameters in Photovoltaic Cells Utilizing Multi-Strategy Fusion Slime Mould Algorithm

**CHI CHEN[1], XIAN CHEN[2], AND AIJU LIN[3]**
[1]School of Data Science and Artificial Intelligence, Wenzhou University of Technology, Wenzhou 325000, China
[2]Wenzhou Polytechnic, Wenzhou, Zhejiang 325035, China
[3]College of International Education, Wenzhou University, Wenzhou, Zhejiang 325035, China

Corresponding authors: Xian Chen (2015021111@wzpt.edu.cn) and Aiju Lin (linaiju123@126.com)

**ABSTRACT** The study presents the Multi-Strategy Learning Fusion Slime Mould Algorithm (MFSMA), a novel method designed to optimize parameters in photovoltaic systems, thereby increasing the efficiency of solar energy conversion. MFSMA employs an advanced technique that incorporates elite opposition-based learning to quickly identify optimal solutions while preserving diversity within the population. Additionally, it integrates a ranking mechanism from the Grey Wolf Algorithm, which categorizes individuals according to their fitness levels, ensuring a balanced approach between exploratory diversity and exploitative precision during the optimization journey. Through rigorous testing on various benchmark functions, MFSMA has demonstrated its exceptional ability to outperform existing algorithms widely used in the sector. The algorithm's effectiveness is further validated through its application in determining the parameters of single, double, and triple-junction photovoltaic modules. Moreover, the durability and effectiveness of the MFSMA algorithm have been rigorously evaluated using data from manufacturers' datasheets across different temperature and irradiance conditions. Statistical analysis supports the conclusion that MFSMA offers superior accuracy and dependability in estimating vital parameters for photovoltaic modules, making it an invaluable tool for overcoming the challenges of parameter identification in solar energy technologies.

**INDEX TERMS** Photovoltaic models, parameter extraction, slime mould algorithm, multi-strategy learning, parameter optimization, grey wolf algorithm, elite opposition-based learning.

## I. INTRODUCTION

As the repercussions of the conflict between Russia and Ukraine spread globally and the energy crisis intensifies, some nations are responding by doubling their investments in fossil fuels [1]. Billions are being funneled into the coal, oil, and natural gas industries, which are principally responsible for exacerbating the climate crisis [2]. Concurrently, all climate indicators are relentlessly setting new records, foretelling that large areas of the Earth will soon experience severe storm surges, floods, droughts, wildfires, and unbearable heatwaves. The world is on the precipice of climatic chaos. Persisting on directing more funds toward the exploration and production of fossil fuels demonstrates a stubborn refusal to recognize our mistakes. Fossil fuels are not the answer to this problem, nor will they ever be. The damage we have inflicted on Earth and its societies is starkly evident, with relevant news emerging daily, and no one is impervious to these impacts. Fossil fuels are a principal cause of the climate crisis; the solution lies in renewable energy. This alternative has the capacity to limit environmental degradation and bolster energy security. A plethora of sustainable energy sources are at our disposal, including geothermal, wind, and notably, solar energy. Solar

The associate editor coordinating the review of this manuscript and approving it for publication was Jiang Wu.

energy bears substantial potential as the preeminent clean energy source for widespread use. Firstly, the distribution of solar energy is extensive across the globe. The sun's radiance uniformly illuminates Earth's surface, irrespective of geographical region, making it exploitable on land or sea, mountainous terrains, or flatlands alike. Secondly, the energy conversion process involved in photovoltaic power generation is straightforward and subjects itself to minimal energy losses. Photovoltaic power generation excludes the necessity of intermediate processes such as the conversion of thermal energy to mechanical energy, or mechanical energy to electromagnetic energy [3], [4]. Furthermore, this process obviates mechanical movements, thereby eliminating mechanical wear and tear. Consequently, photovoltaic power generation touts a high theoretical power generation efficiency and holds considerable potential for technological advancements. Nonetheless, numerous challenges need to be addressed within solar photovoltaic systems. For instance, photovoltaic power generation can be impacted by factors such as weather conditions, seasonal variations, and radiation intensity. During prolonged rain spells or in certain extreme regions, photovoltaic systems may generate scant or even no electricity. Moreover, as the duration of usage of photovoltaic systems extends, inevitable hardware deterioration occurs, directly influencing the system's stable operation. Consequently, it is crucial to design and optimize photovoltaic systems effectively and to accurately evaluate their practical performance [5], [6].

The practical performance of a photovoltaic (PV) system is contingent upon the relevant unknown parameters. Evaluating these parameters can enhance our comprehension of the PV system's real-world performance [7]. Nonetheless, a multitude of challenges persist within solar photovoltaic (PV) systems that necessitate attention. Factors such as weather variability, seasonal changes, and fluctuating radiation intensity significantly impact photovoltaic power generation. During extended rainy periods or within particularly harsh environments, PV systems may produce minimal or even no electricity at all. Moreover, with the ongoing utilization of PV systems, hardware degradation becomes an inevitable consequence, adversely impacting the stability and operational reliability of the system. Consequently, it is imperative to adeptly design and optimize PV systems, as well as accurately evaluate their real-world performance. The operational efficiency of a PV system in practice hinges on various unknown parameters. A thorough assessment of these parameters can offer a more comprehensive understanding of the system's actual performance. However, standard diode model (SDM), double diode model (DDM), triple diode model (TDM), and PV system equations often manifest as implicit transcendental equations, rendering the parameter extraction process exceptionally challenging. Hence, devising an effective method for extracting these unknown parameters has become a focal point for continued research and study. Consequently, effective methods for extracting unknown parameters become the focal point for subsequent research [8].

Swarm Intelligence (SI) algorithms have garnered significant attention from researchers due to their wide-ranging applicability, absence of black-box issues, lack of stringent mathematical requirements such as differentiability for problem-solving, and their ability to locate near-optimal solutions in a reasonable timeframe without necessitating gradient computation. Their exploratory and exploitative tendencies have been extensively studied in various fields, encompassing areas such as economic emission dispatch problems, image segmentation, scheduling issues, medical diagnosis, costly optimization challenges, feature selection, and global optimization. As a result, recent years have witnessed the emergence of innovative and groundbreaking algorithms, such as the Slime Mould Algorithm (SMA) [9], Harris Hawks Optimization (HHO) [10], Hunger Games Search (HGS) [11], Runge-Kutta Optimizer (RUN) [12], Colony Predation Algorithm (CPA) [13], Weighted Mean of Vectors (INFO) [14], and Grey Wolf Algorithm [15]. Recently, these SIs algorithms have been applied in identifying parameters of several photovoltaic models to optimize the efficiency of photovoltaic models for maximum conversion of solar energy into electrical energy. Song et al. [16] developed a multi-strategy, co-evolutionary differential evolution algorithm (MPPCEDE) designed to fine-tune photovoltaic model parameters, thereby enhancing the conversion efficiency of solar energy into electricity. Chen et al. [17] introduced an innovative perturbed stochastic fractal search algorithm that employs both a perturbed stochastic fractal search operator and a chaotic elite perturbation strategy for the precise optimization of parameters within photovoltaic systems. Yousri et al. [18] leveraged a fractional-order chaotic map variant (FCmap) to boost the parameter extraction capabilities of the Enhanced Particle Swarm Optimization (EPSO) [19]. Dkhichi et al. [20] amalgamated the Levenberg–Marquardt (LM) approach with simulated annealing (SA) [21], proposing the LMSA method to counteract the detrimental effects of photovoltaic model degradation. Li et al. [22] enhanced the sparrow search algorithm (SSA), formulating a quantum adaptive version that demonstrated impressive outcomes in isolated island microgrids. Abbassi et al. [23] refined DDM parameters utilizing the salp swarm algorithm [24]. Although meta-heuristic algorithms have showcased remarkable performance in practice, they are not without their challenges. Primarily, the quality of solutions and convergence velocity invite further enhancement. Secondly, following the no-free-lunch theorems [25], algorithmic approaches require bespoke analyses tailored to specific problems, compelling ongoing research, and the development of more sophisticated algorithms suited to varying problem domains.

This study is dedicated to advancing a multi-strategy fusion Slime Mould Algorithm (MFSMA), which incorporates an opposition-based learning operator and the operators from

the Grey Wolf Optimizer (GWO) to enhance the evaluation of photovoltaic models. SMA is inspired by the natural behavior of slime mould, particularly its ability to find the shortest path between points in a network, which mirrors the process of optimizing solutions. This bio-inspired algorithm stands out for its simplicity in implementation, flexibility in handling multi-dimensional and multi-objective problems, and robustness against local optima traps. Compared to other algorithms, SMA often requires fewer parameters to be adjusted, making it more user-friendly and less prone to overfitting. Its capability to dynamically adapt to the changing landscape of a problem space ensures a good balance between exploration and exploitation, leading to high-quality solutions within shorter computational times. These characteristics make SMA a compelling choice for tackling a wide range of optimization challenges where traditional algorithms might struggle. Within MFSMA, these two mechanisms synergize to yield superior optimization outcomes. Addressing one primary limitation of the current Swarm Intelligence (SI) algorithms—the paucity of inter-individual communication within the population—an opposition-based learning mechanism has been integrated. This innovative approach not only compensates for insufficient interaction amongst population members but also adeptly circumvents local optima, thereby fortifying the algorithm's capability for local exploitation. In pursuit of a more expansive solution space that enables broader search capabilities, the GWO mechanism was incorporated. The amalgamation of these mechanisms empowers MFSMA with robust solution-finding efficiency while simultaneously equipping it with the agility to escape local optimality traps. To validate the efficacy and reliability of this proposed method, comparative analyses are conducted against other cutting-edge algorithms, alongside comprehensive experimentation on multimodal problems related to assessing unknown parameters in photovoltaic models. The empirical evidence suggests that MFSMA exhibits commendable performance in tackling photovoltaic optimization challenges.

The main contributions are as follows:

- To enhance the extraction of unknown parameters across diverse photovoltaic modules, the multi-strategy fusion Slime Mould Algorithm has been refined and designated as the MFSMA.
- Inter-individual communication within a population is bolstered through the integration of an opposition-based learning operator as a search mechanism.
- A Grey Wolf Optimizer (GWO) operator is incorporated to facilitate exploration within an expanded solution space in MFSMA.
- A comparative analysis of MFSMA against leading algorithms confirms its substantial competitive strength in the evaluation of photovoltaic model challenges.
- The proficiency of MFSMA in parameter extraction within intricate environments is rigorously evaluated.

The organization of this document is outlined as follows: Section II delineates the particulars of background. Section III offers an in-depth exposition of the MFSMA algorithm. Numerical outcomes are disclosed in Section IV, with Section IV-A detailing the validation benchmarks for MFSMA. The application results of MFSMA to the Standard Diode Model (SDM), Double Diode Model (DDM), and photovoltaic modules are encapsulated in Section IV-B. Section IV-C presents the performance of MFSMA against the manufacturer's datasheet specifications. A comprehensive discussion is situated in Section V, and concluding remarks along with prospective avenues for research are situated in Section VI.

## II. PROBLEM FORMULATION

### A. SINGLE DIODE MODEL (SDM)

The equivalent circuit model of a Sigma-Delta Modulator (SDM) is depicted in Figure 1. Owing to its relatively straightforward architecture, this model enjoys widespread utilization. It is characterized by a mere five parameters. Photogenerated current, sometimes referred to as induced current, denotes the flow of electrical charge driven by carriers that are excited into motion within the battery under photonic stimulation. This current is deeply intertwined with the energy band structure of the battery and hinges on the generation rate and the mobility of these photogenerated carriers. The diode reverse saturation current, also known as dark current, can be attributed to the properties like barrier height, the expanse of the depletion layer, and the thermal conditions within the PN junction of the battery. Regarding the diode ideal factor—or emission coefficient—this metric serves to evaluate the extent to which imperfections in the battery influence its capacity for light absorption and the efficacy of photon emission. An elevated ideal factor signifies a heightened degree of carrier recombination within the battery, pointing to efficiency losses. The series resistance is largely derived from the inherent bulk resistance present in semiconductor materials, compounded by the resistive interface formed at the juncture between metal and semiconductor layers. Lastly, the parallel, or shunt, resistance is indicative of the PN junction's suboptimal behaviors within the battery and is illustrative of local short-circuit phenomena, often precipitated by impurities situated proximate to the junction.

The final $I_L$ is calculated as $I_L = I_{ph} - I_{sh} - I_d$, where $I_{ph}$ represents the photogenerated current; $I_{sh}$ denotes the shunt resistor current. $I_d$ is the diode current; $I_L$ is the ultimate current output. $I_d$ is calculated as $I_d = \left[\exp\left(\frac{(V_L+R_s \bullet I_L)}{n \bullet k \bullet T} \bullet q\right) - 1\right] \bullet I_{sd}$, where $I_{sd}$ signifies the reverse saturation current, $q$ represents the charge of an electron, quantified as $(1.60217646 \times 10^{-19})$ Coulombs (C), $V_L$ denotes the output voltage, $R_s$ is the series resistance, and $n$ indicates the diode's ideal coefficient. The constant $k$ has a value of $(1.3806503 \times 10^{-23})$ Joules per Kelvin (J/K). $T$ stands for temperature, measured in Kelvin, which is the temperature unit employed throughout this paper. $I_{sh}$ is $I_{sh} = \frac{V_L+R_s \bullet I_L}{R_{sh}}$,where $R_{sh}$ represents the shunt

resistance, and $V_L$, $R_s$, and $I_L$ denote the same content as previously mentioned. And then the $I_L = I_{ph} - I_{sh} - I_d$ can be wirten as:

$$I_L = I_{pl_r} - I_{sdl} \cdot \left[\exp\left(\frac{q \cdot (V_L + R_S \cdot I_L)}{n \cdot k \cdot T}\right) - 1\right] - \frac{V_L + R_S \cdot I_L}{R_{sh}} \quad (1)$$

where $I_{ph}, I_{sd}, R_s, R_{sh}$ and $n$ are the unknown parameters in SDM, which exert a significant influence on the conversion efficiency of solar energy.

### B. DOUBLE DIODE MODEL (DDM)

In pursuit of heightened accuracy amidst intricate environmental conditions, the Dual Diode Model (DDM) incorporates an additional diode in series with a photovoltaic power source, as compared to the Single Diode Model (SDM). The equivalent circuit representation of DDM is illustrated in Figure 2. $I_L$ is $I_L = I_{ph} - I_{d1} - I_{sh} - I_{d2}$, and then it can also be

$$I_L = I_{ph} - I_{sd1} \cdot \left[\exp\left(\frac{q \cdot (V_L + R_S \cdot I_L)}{n_1 \cdot k \cdot T}\right) - 1\right] - I_{sd2} \cdot \left[\exp\left(\frac{q \cdot (V_L + R_S \cdot I_L)}{n_2 \cdot k \cdot T}\right) - 1\right] - \frac{V_L + R_S \cdot I_L}{R_{sh}} \quad (2)$$

where $n_1$ and $n_2$ signify the ideal coefficients of the diodes; $I_{sd1}$ and $I_{sd2}$ represent the diode diffusion current and reverse saturation current, respectively; other parameters remain consistent with those previously described. $I_{ph}$, $I_{sd1}$,$I_{sd2}$,$R_s$, $R_{sh}$, $n_1$, and $n_2$ are unknown parameters that will impinge upon the performance of the DDM in terms of solar energy conversion efficiency

### C. PV MODULE MODEL

The photovoltaic (PV) module model is composed of solar cells of varying sizes arranged in series or parallel configurations, and its equivalent circuit is depicted in Figure 4. Equations 3 and 4 respectively correspond to the output current expressions for the Single Diode Model (SDM) and Dual Diode Model (DDM) applied to the PV module.

$$I_L = I_{ph}N_p - I_{sd} \bullet N_p \bullet \left[\exp\left(\frac{q \bullet \left(\frac{V_L}{N_s} + N_s \bullet R_s \bullet \frac{I_L}{N_p}\right)}{n \bullet k \bullet N_s \bullet T}\right) - 1\right] - \frac{\frac{V_L}{N_s} + N_s \bullet R_s \bullet \frac{I_L}{N_p}}{\frac{R_{ss} \bullet N_s}{N_p}} \quad (3)$$

$$I_L = I_{ph}N_p - I_{sd11} \bullet N_p \bullet \left[\exp\left(\frac{q \bullet \left(\frac{V_L}{N_s} + N_s \bullet R_s \bullet \frac{I_L}{N_p}\right)}{n_1 \bullet k \bullet T \bullet N_s}\right) - 1\right] - I_{sd2} \bullet N_p \bullet \left[\exp\left(\frac{q \bullet \left(\frac{V_L}{N_s} + N_s \bullet R_s \bullet \frac{I_L}{N_p}\right)}{n_2 \bullet k \bullet T \bullet N_s}\right) - 1\right] - \frac{\frac{V_L}{N_s} + N_s \bullet R_s \bullet \frac{I_L}{N_p}}{\frac{R_{sh} \bullet N_s}{N_p}} \quad (4)$$

where $N_s$ represents the number of solar cells connected in series, and $N_p$ is the number of solar cells connected in parallel. It is evident that $I_{ph}$, $I_{sd}$, $R_s$, $R_{sh}$, and $n$ are the unknown parameters.

### D. OBJECTIVE FUNCTION

From the aforementioned discussion, our objective is to ensure that the derived values of $I_L$ and $V_L$ closely approximate actual conditions. To quantify this accuracy, we employ the Root Mean Square Error (RMSE) as a metric, with the calculation formula presented as follows:

$$RMSE(X) = \sqrt{\frac{1}{N}\sum_{i=1}^{N} f_i^2\,(V_L, I_L, X)} \quad i = 1, 2, \ldots, \mathrm{N} \quad (5)$$

where $X$ symbolizes the vector of the parameter set; popsize denotes the number of measured current data points. For the SDM, DDM, and TDM, $X$ encompasses the unknown parameters that influence their respective performances.

$$f\,(V_L, I_L, X) = I_{ph} - I_L - I_{sd} \bullet \left[\exp\left(\frac{q \bullet (V_L + R_s \bullet I_L)}{n \bullet k \bullet T}\right) - 1\right] - \frac{V_L + R_s \bullet I_L}{R_{sh}} \quad (6)$$

$$f\,(V_L, I_L, X) = I_{ph} - I_L - I_{sd1} \bullet \left[\exp\left(\frac{q \bullet (V_L + R_s \bullet I_L)}{n_1 \bullet k \bullet T}\right) - 1\right] - I_{sd2} \bullet \left[\exp\left(\frac{(R_s \bullet I_L + V_L)}{k \bullet T \bullet n_2} \bullet q\right) - 1\right] - \frac{V_L + R_s \bullet I_L}{R_{sh}} \quad (7)$$

$$f\,(V_L, I_L, X) = I_{ph} - I_{sd1} \bullet \left[\exp\left(\frac{q \bullet (V_L + R_s \bullet I_L)}{n_1 \bullet k \bullet T}\right) - 1\right] - I_{sd2} \bullet \left[\exp\left(\frac{q \bullet (V_L + R_s \bullet I_L)}{n_2 \bullet k \bullet T}\right) - 1\right] - I_{sd3} \bullet \left[\exp\left(\frac{q \bullet (V_L + R_s \bullet I_L)}{n_3 \bullet k \bullet T}\right) - 1\right] - \frac{V_L + R_s \bullet I_L}{R_{sh}} - I_L \quad (8)$$

## III. THE PROPOSED ALGORITHM

### A. SLIME MOULD ALGORITHM

Drawing on the oscillatory behavior observed in natural slime mould, the newly developed Slime Mould Algorithm (SMA) boasts a set of unique features encapsulated within an advanced mathematical framework. The model is predicated

on adaptive weighting strategies that mirror the dynamic feedback processes found in the wave propagation patterns of slime mould, orchestrated by a bio-oscillator. This sophisticated algorithm demonstrates exceptional proficiency in establishing optimal foraging paths, evidencing superior explorative prowess and an inclination toward effective resource utilization. Since the SMA was proposed, it has received widespread attention in academia and engineering application circles [9].

The slime mold exhibits chemotactic behavior by moving toward a food source in response to olfactory cues. The contraction mechanism of the slime mold as it approaches the nutrient can be represented by the following mathematical models:

$$\overrightarrow{X(t+1)} = \begin{cases} \overrightarrow{X_b(t)} + \overrightarrow{vb} \cdot \left(\vec{W} \cdot \overrightarrow{X_A(t)} - \overrightarrow{X_B(t)}\right), & r < p \\ \overrightarrow{vc} \cdot \overrightarrow{X(t)}, & r \geq p \end{cases} \tag{9}$$

where $\overrightarrow{vb}$ represents some sort of velocity or change in position that is bounded between negative a and positive a, $t$ often indexes the current step or generation in the process,$\overrightarrow{X_b}$ represents the individual location with the highest odour concentration currently found, $\overrightarrow{X}$ represents the location of slime mould, $\overrightarrow{X_A}$ and $\overrightarrow{X_B}$ represent two individuals randomly selected from the slime mould population, and $\vec{W}$ can affect how different components of the model influence the outcome. The mathematical formula for updating the location of slime mould is as follows:

$$\overrightarrow{X^*} = \begin{cases} \text{rand} \cdot (UB - LB) + LB, & \text{rand} < z \\ \overrightarrow{X_b(t)} + \overrightarrow{vb} \cdot \left(W \cdot \overrightarrow{X_A(t)} - \overrightarrow{X_B(t)}\right), & r < p \\ \overrightarrow{vc} \cdot \overrightarrow{X(t)}, & r \geq p \end{cases} \tag{10}$$

This snippet generates a random value within the range defined by $LB$ and $UB$, $rand$ and $r$ denote the random value in [0,1]. The detailed description can be seen in Algorithm 1. The input parameters are population size $n$, current iteration number $t$, maximum iterations $T$, and dimension $d$. In lines two to five of the algorithm, each individual within the population is randomly generated, thereby completing the initialization of the population $X = \{x_1, X_2, X_3, \ldots, X_n\}$. In lines seven to thirteen of the algorithm, the algorithm enters the iterative optimization process. If the current iteration count $t$ is less than the maximum number of iterations $T$, the algorithm continues to execute. If the current iteration count exceeds the number of iterations, then the algorithm completes and produces the output $F_b$ and $X_{best}$. During the iterative optimization process, it is necessary to perform operations such as calculating the fitness for each individual and updating their positions accordingly.

**Algorithm 1** Slime Mould Algorithm(SMA)

**Input:** $n$: Population Size;
$t$: Current Iteration Number;
$T$: Maximum iterations;
$d$: Dimension;
**Output:** best fitness $F_b$; $X_{best}$

1 $t \leftarrow 0$;
2 **for** $i = 1$ **to** $n$ **do**
3  **for** $j = 1$ **to** $d$ **do**
4  $X_{ij} \leftarrow$ Initialization(i,j);
5  $X_i \leftarrow \{x_{i1}, x_{i2}, x_{i3}, \ldots, x_{id}\}$;
6 $X \leftarrow \{x_1, X_2, X_3, \ldots, X_n\}$;
7 **while** *NotTermination*($t < T$) **do**
8  **for** $i = 1$ **to** $n$ **do**
9  $F_i \leftarrow$ fitness($X_i$);
10  Update the best fitness $F_b$;;
11  **for** $i = 1$ **to** $n$ **do**
12  Update the position of $X_i$;
13  $t \leftarrow$t+1;
14 **return** $F_b$; $X_{best}$.

### B. GREY WOLF ALGORITHM

The Grey Wolf Optimizer (GWO) algorithm emulates the hierarchical mechanism of leadership and hunting behaviors observed in natural grey wolf packs. It simulates social hierarchy through four types of grey wolves and mimics the predatory actions of tracking, encircling, pursuing, and attacking prey to fulfill the goal of optimization search. The GWO algorithm is characterized by its simplicity of principle, inherent parallelism, ease of implementation, minimal requirement for parameter tuning, and independence from gradient information of the problem, along with a robust capability for global search [15]. In the GWO algorithm, an initial population of grey wolves is generated randomly within the search space. To construct a model of the social hierarchy, the fittest solution in the population is designated as the alpha ($\alpha$) wolf, the second-best as the beta ($\beta$) wolf, and the third-best as the delta ($\delta$) wolf, while the rest are considered omega ($\omega$) wolves. Guided by the $\alpha$, $\beta$, and $\delta$ wolves, the $\omega$ wolves follow and participate in the hunting optimization process, which involves searching for, encircling, and attacking prey, culminating in the identification of the optimal solution.

To mathematically model the hunting behavior of grey wolves, we posit that the alpha (optimal candidate solution), along with the beta and delta, possess superior knowledge regarding the potential location of the prey. Consequently, we retain the top three solutions discovered to date, compelling the remaining search agents (comprising the omegas) to adapt their positions in accordance with those of the leading search agents. In alignment with this concept, we introduce the following formulas. The core components of the GWO algorithm are as follows:

$$\vec{D}_\alpha = \left|\vec{C}_1 \cdot \vec{X}_\alpha - \vec{X}\right|, \vec{D}_\beta = \left|\vec{C}_2 \cdot \vec{X}_\beta - \vec{X}\right|,$$

$$\begin{aligned}
\vec{D}_\delta &= \left|\vec{C}_3 \cdot \vec{X}_\delta - \vec{X}\right| \\
\vec{X}_1 &= \vec{X}_\alpha - \vec{A}_1 \cdot \left(\vec{D}_\alpha\right), \vec{X}_2 = \vec{X}_\beta - \vec{A}_2 \cdot \left(\vec{D}_\beta\right), \\
\vec{X}_3 &= \vec{X}_\delta - \vec{A}_3 \cdot \left(\vec{D}_\delta\right) \\
\vec{X}(t+1) &= \frac{\vec{X}_1 + \vec{X}_2 + \vec{X}_3}{3}
\end{aligned} \tag{11}$$

where $t$ is the current number of iterations,the $\vec{D}_\alpha$, $\vec{D}_\beta$ and $\vec{D}_\delta$ are the distance between the $\alpha$ wolf, $\beta$ wolf, $\delta$ wolf between the current selected wolf. The $\vec{A}_1$, $\vec{A}_2$, $\vec{A}_3$ and $\vec{C}_1$, $\vec{C}_2$, $\vec{C}_3$ are the coefficient vectors. The $\vec{X}_\alpha$, $\vec{X}_\beta$, and $\vec{X}_\delta$ are the position vector of the prey. In this study, we attempt to integrate the core operators of the Grey Wolf Optimizer (GWO) algorithm with an opposition-based learning strategy into the original Sine Cosine Algorithm (SMA), to integrate the core operators of the Grey Wolf Optimizer (GWO) algorithm with an opposition-based learning strategy into the original Sine Cosine Algorithm (SMA).

### C. THE OPPOSITION-BASED LEARNING

Over the past decade, Opposition-Based Learning (OBL) has emerged as a distinctive research domain garnering considerable attention [26], [27]. The OBL concept has been leveraged to boost numerous soft computing algorithms, including Reinforcement Learning (RL), Artificial Neural Networks (ANN), Fuzzy Systems, and various optimization methods like Genetic Algorithms (GA). The opposite number of OBL is defined as follows: the $x \in [a, b]$ be a real number and its opposite $\breve{x}$ is $\breve{x} = a + b - x$ if the opposite point in the $D$ space $x_i \in [a_i, b_i]$ , $i = 1, 2, \ldots, D$, the opposite of $x$ is $\breve{x}$ $(\breve{x}_1, \ldots, \breve{x}_D)$ and $\breve{x}_i = a_i + b_i - x_i$ [28].

Elite opposition-based learning (EOBL) is an avant-garde methodology in the realm of computational intelligence, as recently introduced in [29]. Within EOBL, elite individuals are initially identified to generate elite opposition solutions that correspond to the current solutions. By evaluating and comparing these elite opposition solutions with the existing ones, the most advantageous individuals are selected to constitute the succeeding generation. This strategy not only broadens the algorithm's exploratory scope but also amplifies the population's diversity and augments the efficacy of the optimization algorithm. In this research, we integrate an elite opposition-based learning strategy with the core operators of the Grey Wolf Optimizer (GWO) into the original Sine Cosine Algorithm (SMA), with the expectation of enhancing the performance of the existing SMA algorithm.

### D. THE PROPOSED MFSMA

In this study, we delineate a novel methodological framework MFSMA wherein the core components of the GWO algorithm are intricately woven together with the principles of elite opposition-based learning. By embedding this composite strategy within the fabric of the original SMA, we intend to cultivate a hybridized algorithmic entity. This enhanced entity is anticipated to not only inherit the powerful search capabilities intrinsic to GWO—characterized by its mimicking of grey wolves' social hierarchy and hunting techniques—but also to gain from the dynamic and innovative features of opposition-based learning. Elite opposition-based learning introduces a paradigm where solutions are not merely considered in isolation but are also evaluated against their diametric counterparts within the solution space. This conceptual leap encourages the algorithm to contemplate alternative perspectives and thereby avoid premature convergence on local optima, a frequent pitfall in complex optimization problems. The integration is meticulous and deliberate, ensuring that the adaptive mechanisms that govern the wolves' pursuit, encirclement, and eventual capture of prey in GWO are harmoniously balanced with the reflective and explorative impetus provided by opposition-based learning. When enmeshed with SMA's mathematical elegance—its sinusoidal functions guiding search agents through a balance of exploration and exploitation—the result is an algorithm poised for robust performance. The detailed description of the MFSMA is shown in Algorithm 2. The input parameters are $n$, $t$, $T$, and $d$. The population $X = \{X_1, X_2, X_3, \ldots, X_n\}$ is generated at line five and the $i^{th}$ individual is $X_i$. Line six initializes the value of $t$ to 0. While the maximum number of iterations $T$ is greater than the current iteration count $t$, the algorithm MFSMA enters the iterative loop. And the position of each individual is updated by the original SMA. During the iterative optimization process, each individual is updated using GWO operators at the $17^{th}$ line. If the current iteration count exceeds the number of iterations, then the algorithm completes and produces the output $F_b$ and $X_{best}$.

## IV. NUMERICAL RESULTS

An in-depth evaluation of the MFSMA method was carried out via three separate trials in this study. To begin, some benchmarks were performed to measure whether the MFSMA's property with the multi-strategy learning operators was significantly better than that of the traditional SMA. There are seven unimodal tasks (F1-F7), six multimodal tasks (F8-F13), and ten different fixed-dimension multimodal tasks (F14-F23) [30]. Unlike unimodal tasks, which only have a single global ideal, multimodal and fixed-dimension multimodal tasks often have more than one local optimal value for assessing the exploratory attribute. In addition, MFSMA was compared to other current algorithms including BA [31], PSO [32], FA [33], and GSA [34]. The parameters of these algorithms are shown in Table 1.

In the second phase of our study, the MFSMA is deployed to optimize parameter estimation for various types of solar cells, including SDM, DDM, and encapsulated PV modules. This investigation maintains consistency by employing the same computational framework and conditions as previous studies, with the bounds of the parameters delineated in Table 2 for comparative analysis. Moreover, we benchmarked the performance of MFSMA against several meticulously selected algorithms that have demonstrated efficacy in similar

**Algorithm 2** Multi-Strategy Learning Fusion Slime Mould Algorithm (MFSMA)

**Input:** $n$: Population Size;
$t$: Current Iteration Number;
$T$: Maximum iterations;
$d$: Dimension;
**Output:** best fitness $F_b$; $X_{best}$

**for** $i = 1$ **to** $n$ **do**
  **for** $j = 1$ **to** $d$ **do**
    $X_{ij} \leftarrow$ Initialization(i,j);
  $X_i \leftarrow \{x_{i1}, x_{i2}, x_{i3}, \ldots, x_{id}\}$;
$X \leftarrow \{x_1, X_2, X_3, \ldots, X_n\}$;
$t \leftarrow 0$;
**while** *NotTermination*($t < T$) **do**
  **for** $i = 1$ **to** $n$ **do**
    $F_i \leftarrow$ fitness($X_i$);
  Update the best fitness $F_b$;;
  **for** $i = 1$ **to** $n$ **do**
    Update the position of $X_i$;
  $X_* \leftarrow$ sort($X$); $X_\alpha \leftarrow X_*(1)$;
  $X_\beta \leftarrow X_*(2)$; $X_\delta \leftarrow X_*(3)$;
  Calculate the $\vec{X}_1$,$\vec{X}_2$,$\vec{X}_3$;
  **for** $i = 1$ **to** $n$ **do**
    Update the $i^{th}$*individual* using GWO operator;
    Calculated the opposite position of the $i^{th}$*individual*;
  $t \leftarrow$t+1;
**return** $F_b$; $X_{best}$.

contexts. These include NPSOPC as reported by Lin and Wu [35], BLPSO introduced by Liang et al. [36], CLPSO detailed comprehensively by Liang et al. [36], GOTLBO as outlined by Chen et al. [37], and EMSFLA evaluated by Wang et al. [38]. Each of these established methods serves as a competitor in assessing the effectiveness of the proposed approach.

In this research, the Wilcoxon signed-rank test is implemented with a significance level of 0.05 to ascertain the comparative performance of the MFSMA. Symbols '+', '−', and '=' are employed to denote instances where MFSMA outperforms, underperforms, or matches the performance of its counterparts respectively. To rigorously evaluate MFSMA's robustness under extreme conditions, such as high pressure or low temperatures, one practical dataset is sourced from manufacturer specifications. This analysis also encompasses scenarios with varying levels of irradiance and temperature, ensuring a comprehensive assessment of the algorithm's adaptability. The execution of MFSMA and competing algorithms takes place on the MATLAB R2020b platform, throughout thirty independent trials, thereby mitigating any randomness in the testing process. The computations are conducted on a computer equipped with an Intel(R) Core(TM) i7-7500U CPU at 2.70GHz and 8.00 GB of RAM. For these photovoltaic scenarios, the evolutionary process is run until reaching the maximum iteration count of $1 \times 10^4$, with each agent's fitness determined by the value of the root mean square error (RMSE).

### A. F1-F23 VALIDATION

In this segment of our study, the MFSMA is evaluated against other leading-edge algorithms, namely the original SMA, BA, PSO, FA, and GSA. The benchmark suite encompasses seven unimodal functions (F1-F7), six multimodal functions (F8-F13), and ten fixed-dimension multimodal tasks (F14-F23). Table 3 collates the average results (Avg), standard deviations (STD), and overall rankings for tackling functions F1 through F23, based on 30 independent runs for each algorithm. Examination of this table reveals that the MFSMA consistently achieves superior mean values across the majority of the benchmark tests when competing against these advanced algorithms. Focusing specifically on the unimodal benchmarks, MFSMA not only secures the most favorable mean values but also outshines its contemporaries in terms of standard deviation (STD), suggesting its potent capability in addressing optimization problems characterized by a singular global optimum. This affirms the efficacy of MFSMA's multi-strategy learning mechanisms, which provide a tangible enhancement over the original SMA for unimodal tasks. When navigating the multimodal benchmarks, although MFSMA and SMA exhibit comparable performance, MFSMA still manages to surpass all rivals, further cementing its dominance in these tests. With regard to the fixed-dimension multimodal tasks, MFSMA demonstrates a pronounced superiority, distinctly advancing beyond the capabilities of previous algorithms tailored for such complex multimodal environments. It can also be seen from Table 3, MFSMA performs the best Wilcoxon signed-rank test '-' Compared to other algorithms. In addition, Table 4 shows the detailed Wilcoxon signed-rank test results for each function. It can be seen that the proposed MFSMA has the best rank among all these functions, and the values of mean rank are 1.2173913,2,3.0434783,3.7391304,5.6521739 and 5.2173913 respectively. The overall rank result is that MFSMA still has the best rank among these algorithms.

### B. SOLAR ENERGY CONVERSION SYSTEM RESULTS

#### 1) SDM

Figures 1 and 2 illustrate the I-V and P-V fitting curves derived from the MFSMA model for SDM analysis. The modeled I-V and P-V trajectories demonstrate notable alignment with the experimental data across the entire assessed voltage spectrum. Error-index evaluations, as reflected by the IAE and RE figures in Figures 3 and 4, quantify the precision of the calculated electric current and the fidelity of the simulation. The IAE is established to be below 9.348978932E-03, while the RE metrics range from -5.654789E-02 to

**TABLE 1.** The parameters of these algorithms.

| Paramters | Algorithms | | | | | |
|---|---|---|---|---|---|---|
| | **MFSMA** | **SMA** | **BA** | **PSO** | **FA** | **SA** |
| Population Size | 100 | 100 | 100 | 100 | 100 | 100 |
| Maximum iterations | $1 \times 10^4$ | $1 \times 10^4$ | $1 \times 10^4$ | $1 \times 10^4$ | $1 \times 10^4$ | $1 \times 10^4$ |
| z | 0.03 | 0.03 | / | / | / | / |
| r | [0,1] | [0,1] | / | / | / | / |
| vc | [0,1] | [0,1] | / | / | / | / |
| A | [-a,a], a=2>0 | / | / | / | / | / |
| C | [0,2] | / | / | / | / | / |
| Af | / | / | 0.9 | / | / | / |
| Rf | / | / | 0.8 | / | / | / |
| r0 | / | / | 0.7 | / | / | / |
| w | / | / | / | 0.3 | / | / |
| c1 | / | / | / | [0,1] | / | / |
| c2 | / | / | / | [0,1] | / | / |
| gamma | / | / | / | / | 1 | / |
| beta0 | / | / | / | / | 1 | / |
| alpha | / | / | / | / | 0.2 | / |
| alpha_damp | / | / | / | / | 0.98 | / |
| G0 | / | / | / | / | / | 100 |
| r1 | / | / | / | / | / | 1 |
| K | / | / | / | / | / | 0.2 |
| dt | / | / | / | / | / | 2 |

**TABLE 2.** Parameters of PV cells.

| Parameters | SDM/DDM | | PV module | |
|---|---|---|---|---|
| | Lower | Upper | Lower | Upper |
| $I_{ph}$( A) | 0 | 1 | 0 | 2 |
| $I_{sd}, I_{sd1}, I_{sd2}(\mu A)$ | 0 | 1 | 0 | 50 |
| $R_s(\Omega)$ | 0 | 0.5 | 0 | 2 |
| $R_{\mathrm{sh}}(\Omega)$ | 0 | 100 | 0 | 2000 |
| $n, n_1, n_2$ | 1 | 2 | 1 | 50 |

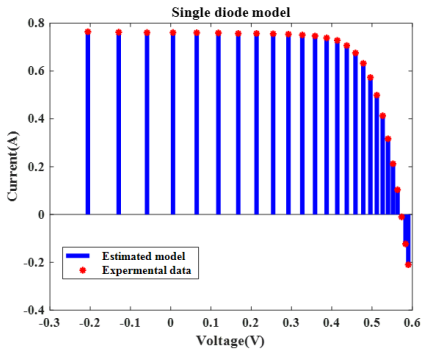


**FIGURE 1.** MFSMA for SDM (I–V characteristics).

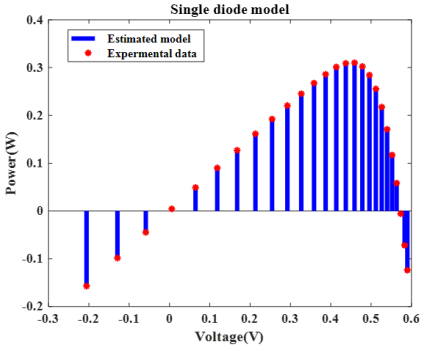


**FIGURE 2.** MFSMA for SDM (P–V characteristics).

1.2898998E+00, suggesting that the MFSMA proficiently captures the authentic properties of SDM. Furthermore, as detailed in Table 5, an absolute individual error of 0.1058408 was recorded, alongside a cumulative discrepancy of 0.0413232 between the experimental findings and the resultant model data. These findings attest to the ability of MFSMA not only to accurately delineate critical SDM parameters but also to offer robust support for further research into this area.

Table 6 summarises the results of 30 separate runs utilizing MFSMA and other competing algorithms. In Table 6, the symbols of the Sig means that the significance of statistical differences among all comparative algorithms after 30 comparative experiments. As can be seen, the

**TABLE 3.** Results of benchmark functions.

| Algorithms | F1 | | F2 | | F3 | | F4 | | F5 | |
|---|---|---|---|---|---|---|---|---|---|---|
| | mean | STD | mean | STD | mean | STD | mean | STD | mean | STD |
| MFSMA | **4.2343434E-27** | **1.02938232E-26** | **1.0092E-13** | **1.001221E-13** | **4.02982323** | **8.4534343** | **2.98938342** | **0.2134533** | **63.4566343** | **36.0392434** |
| SMA | 5.98484E-27(-) | 1.38944E-26(-) | 1.23893E-13(-) | 3.0093E-13(-) | 5.8098738(-) | 9.6098933(-) | 2.5876453(-) | 0.201029383(-) | 64.4879838(-) | 38.8346789(-) |
| BA | 0.78809897(-) | 0.65987337(-) | 400.79837387(-) | 940.0983987(-) | 100.798937(-) | 231.8910197(-) | 25.52092897(-) | 8.12908907(-) | 461.78902727(-) | 361.924567827(-) |
| PSO | 341.738982(-) | 18.778983(-) | 4367038.21(-) | 12801890.33(-) | 2009.71234(-) | 231.2309892829(-) | 6.55789012(-) | 0.50989202(-) | 583389.9808(-) | 82789.39102(-) |
| FA | 27674.06898(-) | 1917.34789(-) | 1675.7410292(-) | 4578.448902(-) | 67493.812902(-) | 6067.519282(-) | 55.709883(-) | 3.06538292(-) | 238938923.34(-) | 6398293.749(-) |
| GSA | 27674.09292(-) | 2.102011(-) | 24.012033(-) | 1.618292(-) | 1908.278904(-) | 354.8908722(-) | 19.782928(-) | 4.087892232(-) | 25324.73929(-) | 8645.678923(-) |

| Algorithm | F6 | | F7 | | F8 | | F9 | | F10 | |
|---|---|---|---|---|---|---|---|---|---|---|
| | mean | STD | mean | STD | mean | STD | mean | STD | mean | STD |
| MFSMA | **4.34323E-27** | **1.54543E-27** | **1.03435E-14** | **2.00323E-13** | **4.7890292** | **8.48786533** | **2.60983942** | **0.1092834** | **63.287953** | **35.8098942** |
| SMA | 1.133442E-26(-) | 3.6232E-26(-) | 0.0567432(-) | 0.0112398(-) | -20072.70098(-) | 414.8239489(-) | 1.908798223(-) | 2.18978645(-) | 2.6457682(-) | 1.2789678(-) |
| BA | 0.6980889(-) | 0.4403934(-) | 75.8907892(-) | 33.4123893(-) | -12266.0394(-) | 728.145793(-) | 515.245678(-) | 42.987383839223(-) | 2.72839232(-) | 0.478934(-) |
| PSO | 345.5238923(-) | 32.7893232(-) | 458.8892892(-) | 60.8909823(-) | -11184.83983(-) | 2843.67892(-) | 701.337839(-) | 35.9897928 (-) | 9.678432 (-) | 0.223782323(-) |
| FA | 27154.87934(-) | 1137.389872(-) | 24.28989332(-) | 3.66893025(-) | -5013.2989783(-) | 442.667832(-) | 477.7908673(-) | 17.548393(-) | 17.126783(-) | 0.3489483(-) |
| GSA | 29.4373883(-) | 2.8765784(-) | 144.189823(-) | 14.4894843(-) | -3288.89829(-) | 513.498983(-) | 388.68983(-) | 13.189823(-) | 4.410923(-) | 0.1783923(-) |

| Algorithm | F11 | | F12 | | F13 | | F14 | | F15 | |
|---|---|---|---|---|---|---|---|---|---|---|
| | mean | STD | mean | STD | mean | STD | mean | STD | mean | STD |
| MFSMA | **4.9893223E-27** | **1.21313E-26** | **1.032313E-13** | **3.008789E-13** | **5.892093232** | **9.67803343** | **2.57896567** | **0.189065443** | **63.365678343** | **34.82345543** |
| SMA | 0.001231762(-) | 0.003894698(-) | 0.904426211(-) | 1.345016196(-) | 0.239508564(-) | 0.070622611(-) | 0.998003838(-) | 0 | 0.000307486(-) | 1.87789E-19(-) |
| BA | 68.48943442(-) | 44.34343432(-) | 14.12895442(-) | 4.9878565(-) | 0.32314677(-) | 0.165678943(-) | 3.1689345(-) | 2.2789655(-) | 0.0012354(-) | 0.00908765(-) |
| PSO | 1.09897897(-) | 0.00876787(-) | 8.1878976(-) | 1.14678965(-) | 714.654678(-) | 756.34575(-) | 3.3345755651(-) | 3.143432567(-) | 0.00111234(-) | 0.000140987(-) |
| FA | 242.567898933(-) | 17.37898738(-) | 20753851.442(-) | 6542063.298(-) | 80548261.3789(-) | 17529188.22(-) | 0.98783928(-) | 0.0003472892(-) | 0.00167893(-) | 0.000498934(-) |
| GSA | 0.527892(-) | 0.05098923(-) | 0.898394834(-) | 0.2898232(-) | 27.3989843(-) | 7.09898564(-) | 1.007892323(-) | 0.022134523(-) | 0.001765644(-) | 0.000498907(-) |

| Algorithm | F16 | | F17 | | F18 | | F19 | | F20 | |
|---|---|---|---|---|---|---|---|---|---|---|
| | mean | STD | mean | STD | mean | STD | mean | STD | mean | STD |
| MFSMA | **4.67895E-28** | **1.25674-26** | **1.019203E-13** | **3.0083E-13** | **5.5673822** | **9.47893872** | **2.5487483** | **0.20348924** | **62.40398423** | **36.4683492** |
| SMA | -1.032897574(-) | 0 | 0.398987453(-) | 0(-) | 3(-) | 0(-) | -3.87987453(-) | 9.489843E-16(-) | -3.2987494(-) | 0.06098943(-) |
| BA(-) | -1.0321987483(-) | 0.000298793(-) | 0.39890932(-) | 0.000357893(-) | 3.04432817843(-) | 0.05678938374(-) | -3.85678392(-) | 0.00810928343(-) | -2.878637264(-) | 0.102938743(-) |
| PSO | -1.0320989746(-) | 0.000839898(-) | 0.40192833(-) | 0.00081237485(-) | 3.08239404(-) | 0.073984738(-) | -3.86689483(-) | 0.0060128394 | -2.889837382(-) | 0.189019283(-) |
| FA | -1.020392321(-) | 0.0001478392(-) | 0.389283222(-) | 0.000467893(-) | 3.02019384(-) | 0.00873684(-) | -3.887283231(-) | 0.000634522(-) | -3.225123412(-) | 0.051345784(-) |
| GSA | -1.0354543(-) | 0.0013232232(-) | 0.39675644(-) | 0.0013452455(-) | 3.02600988(-) | 0.027654567(-) | -3.860456764(-) | 0.001989897(-) | -3.0912345334(-) | 0.0451323278(-) |

| Algorithm | F21 | | F22 | | F23 | | Ranks |
|---|---|---|---|---|---|---|---|
| | mean | STD | mean | STD | mean | STD | |
| MFSMA | **-10.1109231** | **0.098932323** | -7.6789323 | 3.63728922 | **-10.5302923** | **1.00059E-05** | 1 |
| SMA | -10.1212782(-) | 0.10346324(-) | -7.44434534(+) | 3.830034563(+) | -10.537656758(-) | 2.00071E-05(-) | 2 |
| BA | -6.82918923(-) | 2.32109289(-) | -6.600609897(-) | 2.2079223(-) | -7.556738925(-) | 2.89078921(-) | 3 |
| PSO | -3.810292831(-) | 0.743748392(-) | -5.606378932(-) | 1.2312333(-) | -5.47839382(-) | 1.9892821(-) | 4 |
| FA | -6.7893821(-) | 1.2109131(-) | -7.489029382 | 0.70298313 | -7.728392342(-) | 1.16388242(-) | 6 |
| GSA | -4.41029242(-) | 0.987837623(-) | -4.6324489393(-) | 1.689878223(-) | -4.513892842(-) | 1.099983232(-) | 5 |

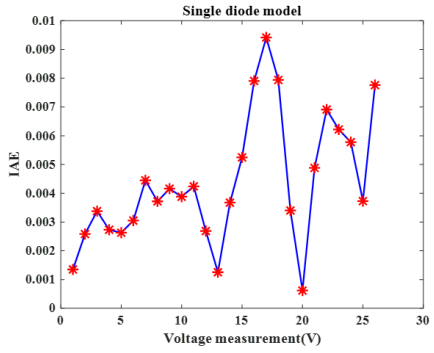


**FIGURE 3.** Error index values on SDM (IAE values).

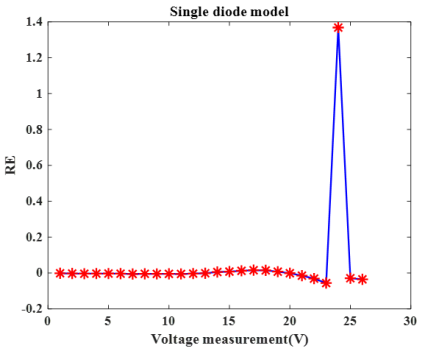


**FIGURE 4.** Error index values on SDM (RE values).

MFSMA proposal has the lowest RMSE values among all comparator sets, indicating that its viability profile is more reliable and consistent than the other algorithms. Using statistical verification data, a significant performance gap

**TABLE 4.** Wilcoxon signed-rank test results.

| Functions | Algorithms | | | | | |
|---|---|---|---|---|---|---|
| | MFSMA | SMA | BA | PSO | FA | GSA |
| **F1** | 1 | 2 | 4 | 3 | 6 | 5 |
| **F2** | 1 | 2 | 3 | 4 | 6 | 5 |
| **F3** | 2 | 1 | 3 | 4 | 6 | 5 |
| **F4** | 1 | 2 | 3 | 4 | 5 | 5 |
| **F5** | 1 | 3 | 2 | 4 | 6 | 5 |
| **F6** | 1 | 2 | 3 | 4 | 6 | 5 |
| **F7** | 1 | 2 | 4 | 3 | 6 | 5 |
| **F8** | 1 | 2 | 3 | 4 | 6 | 4 |
| **F9** | 2 | 1 | 3 | 4 | 6 | 5 |
| **F10** | 1 | 3 | 2 | 4 | 5 | 6 |
| **F11** | 1 | 2 | 4 | 3 | 5 | 5 |
| **F12** | 1 | 2 | 3 | 4 | 6 | 5 |
| **F13** | 2 | 1 | 3 | 4 | 5 | 6 |
| **F14** | 1 | 2 | 3 | 4 | 6 | 5 |
| **F15** | 2 | 1 | 4 | 3 | 6 | 5 |
| **F16** | 1 | 3 | 2 | 4 | 6 | 5 |
| **F17** | 2 | 1 | 4 | 3 | 6 | 5 |
| **F18** | 1 | 3 | 2 | 4 | 5 | 6 |
| **F19** | 1 | 3 | 2 | 4 | 5 | 6 |
| **F20** | 1 | 2 | 3 | 4 | 6 | 5 |
| **F21** | 1 | 2 | 4 | 3 | 5 | 6 |
| **F22** | 1 | 2 | 3 | 4 | 5 | 6 |
| **F23** | 1 | 2 | 3 | 4 | 6 | 5 |
| **Mean** | 1.2173913 | 2 | 3.0434783 | 3.7391304 | 5.6521739 | 5.2173913 |
| **Overall** | **1** | **2** | **3** | **4** | **6** | **5** |

**TABLE 5.** IAE of MFSMA on SDM.

| Number | Measured data | | Simulated current data | | Simulated power data | |
|---|---|---|---|---|---|---|
| | V(V) | I(A) | Isim(A) | IAE1(A) | Psim(W) | IAEp(A) |
| 1 | -0.2057 | 0.764 | 0.76535011 | 0.00135011 | -0.157432518 | 0.000277718 |
| 2 | -0.1291 | 0.762 | 0.764583829 | 0.002583829 | -0.098707772 | 0.000333572 |
| 3 | -0.0588 | 0.7605 | 0.763879766 | 0.003379766 | -0.04491613 | 0.00019873 |
| 4 | 0.0057 | 0.7605 | 0.7632307 | 0.0027307 | 0.004350415 | 1.5565E-05 |
| 5 | 0.0646 | 0.76 | 0.762628983 | 0.002628983 | 0.049265832 | 0.000169832 |
| 6 | 0.1185 | 0.759 | 0.762051336 | 0.003051336 | 0.090303083 | 0.000361583 |
| 7 | 0.1678 | 0.757 | 0.761450788 | 0.004450788 | 0.127771442 | 0.000746842 |
| 8 | 0.2132 | 0.757 | 0.760718919 | 0.003718919 | 0.162185274 | 0.000792874 |
| 9 | 0.2545 | 0.7555 | 0.759659761 | 0.004159761 | 0.193333409 | 0.001058659 |
| 10 | 0.2924 | 0.754 | 0.757879374 | 0.003879374 | 0.221603929 | 0.001134329 |
| 11 | 0.3269 | 0.7505 | 0.754740859 | 0.004240859 | 0.246724787 | 0.001386337 |
| 12 | 0.3585 | 0.7465 | 0.749186415 | 0.002686415 | 0.26858333 | 0.00096308 |
| 13 | 0.3873 | 0.7385 | 0.739754022 | 0.001254022 | 0.286506733 | 0.000485683 |
| 14 | 0.4137 | 0.728 | 0.724324984 | 0.003675016 | 0.299653246 | 0.001520354 |
| 15 | 0.4373 | 0.7065 | 0.701251599 | 0.005248401 | 0.306657324 | 0.002295126 |
| 16 | 0.459 | 0.6755 | 0.667594293 | 0.007905707 | 0.30642578 | 0.00362872 |
| 17 | 0.5119 | 0.499 | 0.495597919 | 0.003402081 | 0.253696575 | 0.001741525 |
| 18 | 0.5265 | 0.413 | 0.413618081 | 0.000618081 | 0.21776992 | 0.00032542 |
| 19 | 0.5398 | 0.3165 | 0.321382154 | 0.004882154 | 0.173482087 | 0.002635387 |
| 20 | 0.5521 | 0.212 | 0.218911229 | 0.006911229 | 0.12086089 | 0.00381569 |
| 21 | 0.5633 | 0.1035 | 0.109719534 | 0.006219534 | 0.061805014 | 0.003503464 |
| 22 | 0.5736 | -0.01 | -0.004222289 | 0.005777711 | -0.002421905 | 0.003314095 |
| 23 | 0.5833 | -0.123 | -0.126729889 | 0.003729889 | -0.073921544 | 0.002175644 |
| 24 | 0.59 | -0.21 | -0.217761054 | 0.007761054 | -0.128479022 | 0.004579022 |
| **Sum of IAE** | / | / | / | **0.096245721** | / | **0.03745925** |

between the proposed SMA-based algorithm and competing algorithms has been demonstrated. A 95% percent certainty level is used to estimate the confidence ranges for the parameter gauges, as shown in Table 7. It's obvious that MFSMA's confidence interval has the best dispersion of any competitor method, indicating that it can successfully disentangle parameters in relatively accurate intermediate intervals.

**TABLE 6.** RMSE of SDM.

| Algorithm | RMSE | | | | | |
|---|---|---|---|---|---|---|
| | Min | Median | Mean | Max | SD | Sig |
| NPSOPC | 7.562311E-04 | 8.526780E-04 | 9.586890E-04 | 9.876789E-04 | 2.355645E-04 | + |
| BLPSO | 1.103042E-03 | 1.573453E-03 | 1.507789E-03 | 2.205389E-03 | 2.544655E-04 | + |
| CLPSO | 1.031456E-03 | 1.074678E-03 | 1.121678E-03 | 1.410234E-03 | 5.566432E-05 | + |
| GOTLBO | 1.333457E-03 | 1.213456E-03 | 1.041079E-03 | 2.363678E-03 | 1.324564E-03 | + |
| EMSFLA | 5.429087E-04 | 4.313213E-04 | 6.213678E-04 | 6.515640E-04 | 1.113454E-06 | + |
| MLCPA | 3.254098E-04 | 3.258990E-04 | 5.421877E-04 | 6.897890E-04 | 1.012457E-06 | + |
| MFSMA | 1.343234E-04 | 2.087660E-04 | 3.245670E-04 | 3.456746E-04 | 9.121234E-07 | |

**TABLE 7.** Confidence intervals on SDM.

| Parameters | Algorithms | | | | | | |
|---|---|---|---|---|---|---|---|
| | NPSOPC | BLPSO | CLPSO | GOTLBO | EMSFLA | MLCPA | MFSMA |
| $I_{ph}$( A) | (0.523 0.696) | (0.533 0.684) | (0.634 0.724) | (0.656 0.755) | (0.762 0.772) | (0.765 0.771) | (0.767 0.770) |
| $I_{sd}(\mu A)$ | (0.201 0.462) | (0.214 0.458) | (0.210 0.432) | (0.293 0.454) | (0.322 0.326) | (0.323 0.327) | (0.323 0.324) |
| $R_S(\Omega)$ | (0.013 0.094) | (0.015 0.056) | (0.019 0.061) | (0.034 0.057) | (0.027 0.038) | (0.027 0.035) | (0.026 0.033) |
| $R_{\mathrm{sh}}(\Omega)$ | (46.53 58.53) | (48.59 57.53) | (48.29 54.55) | (40.53 61.35) | (53.72 54.90) | (53.73 54.78) | (53.74 54.77) |
| $n$ | (1.023 1.673) | (1.033 1.584) | (1.234 1.685) | (1.223 1.352) | (1.113 1.352) | (1.114 1.351) | (1.113 1.340) |

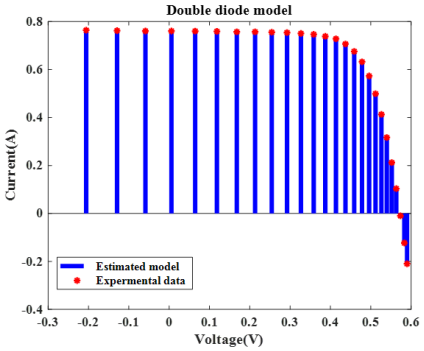


**FIGURE 5.** MFSMA for DDM (I–V characteristics).

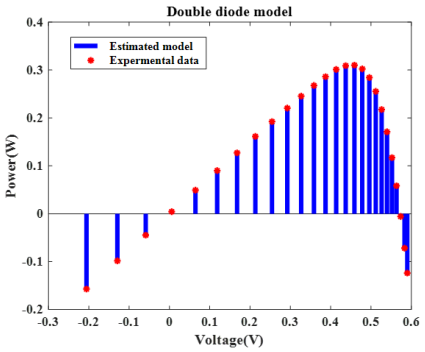


**FIGURE 6.** MFSMA for DDM (P–V characteristics).

### 2) DDM

In this section, the MFSMA is assessed based on its application to the DDM problem. Figures 5 and 6 display the I-V and P-V response characteristics of the MFSMA when applied to DDM. The generated I-V and P-V curves from the proposed technique demonstrate a high degree of congruity with the experimental data across the entire voltage spectrum utilized in this study. Figures 7 and 8 delineate the error indices for the reconstructed electric current and DDM test results, represented by IAE and RE values, respectively. The analysis reveals that the peak IAE value stands at 3.045678E-03, while the upper and lower bounds of the RE values are 2.8658949E-01 and -2.8976723E-02, respectively. These metrics underscore the MFSMA's precision in authentically characterizing the properties of DDM. Additionally, Table 8 details the concrete figures pairing the IAE with the current and control values pertinent to DDM, tallying up to 0.02740828 and 0.010485362, correspondingly. This accuracy enables the unambiguous identification of critical

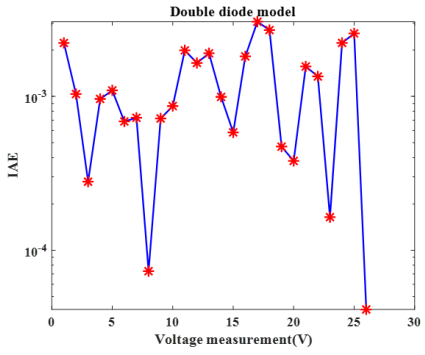


**FIGURE 7.** Error index values on DDM (IAE values).

parameters within DDM and robustly affirms the efficacy of the implemented MFSMA methodology in this context.

Table 9 highlights that MFSMA consistently outshines its contemporaries with respect to root mean square error (RMSE) metrics, recording the lowest (Min), average (Avg), highest (Max), and standard deviation (SD) values. This

**TABLE 8.** IAE of MFSMA on DDM.

| Number | Measured data | | Simulated current data | | Simulated power data | |
|---|---|---|---|---|---|---|
| | V(V) | I(A) | Isim(A) | IAE1(A) | Psim(W) | IAEp(A) |
| 1 | -0.2057 | 0.764 | 0.761773559 | 0.002226441 | -0.156696821 | 0.000457979 |
| 2 | -0.1291 | 0.762 | 0.760964357 | 0.001035643 | -0.098240499 | 0.000133701 |
| 3 | -0.0588 | 0.7605 | 0.760221061 | 0.000278939 | -0.044700998 | 1.64016E-05 |
| 4 | 0.0057 | 0.7605 | 0.75953677 | 0.00096323 | 0.00432936 | 5.49041E-06 |
| 5 | 0.0646 | 0.76 | 0.75890637 | 0.00109363 | 0.049025352 | 7.06485E-05 |
| 6 | 0.1185 | 0.759 | 0.758313143 | 0.000686857 | 0.089860107 | 8.13925E-05 |
| 7 | 0.1678 | 0.757 | 0.757726557 | 0.000726557 | 0.127146516 | 0.000121916 |
| 8 | 0.2132 | 0.757 | 0.757073065 | 7.30649E-05 | 0.123232324 | 1.55774E-05 |
| 9 | 0.2545 | 0.7555 | 0.756218387 | 0.000718387 | 0.161407977 | 0.000198988 |
| 10 | 0.2924 | 0.754 | 0.754865189 | 0.000865189 | 0.136789787 | 0.000232434 |
| 11 | 0.3269 | 0.7505 | 0.740406322 | 0.001906322 | 0.192457579 | 0.000234887 |
| 12 | 0.3585 | 0.7465 | 0.727007442 | 0.000992558 | 0.220722581 | 0.000252981 |
| 13 | 0.3873 | 0.7385 | 0.705916278 | 0.000583434 | 0.286759368 | 0.000738318 |
| 14 | 0.4137 | 0.728 | 0.67368049 | 0.000583722 | 0.300762979 | 0.000410621 |
| 15 | 0.4373 | 0.7065 | 0.628941174 | 0.000598789 | 0.308697188 | 0.000255262 |
| 16 | 0.459 | 0.6755 | 0.689767816 | 0.00181951 | 0.309219345 | 0.000835155 |
| 17 | 0.5119 | 0.499 | 0.570299563 | 0.003058826 | 0.300885458 | 0.001463342 |
| 18 | 0.5265 | 0.413 | 0.498528757 | 0.002700437 | 0.282868583 | 0.001339417 |
| 19 | 0.5398 | 0.3165 | 0.412989078 | 0.000471243 | 0.255196871 | 0.000241229 |
| 20 | 0.5521 | 0.212 | 0.413380477 | 0.000380477 | 0.217644821 | 0.000200321 |
| 21 | 0.5633 | 0.1035 | 0.318065708 | 0.001565708 | 0.171691869 | 0.000845169 |
| 22 | 0.5736 | -0.01 | 0.213347796 | 0.001347796 | 0.117789318 | 0.000744118 |
| 23 | 0.5833 | -0.123 | 0.103664109 | 0.000164109 | 0.058393993 | 9.24425E-05 |
| 24 | 0.59 | -0.21 | -0.12556741 | 0.00256741 | -0.07324347 | 0.00149757 |
| **Sum of IAE** | / | / | / | **0.02740828** | / | **0.010485362** |

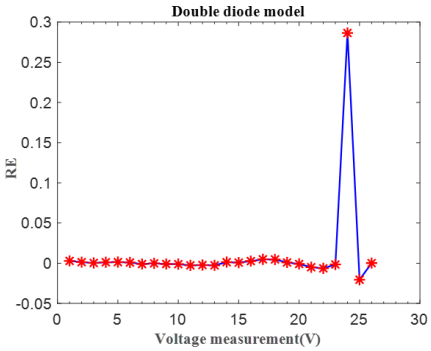


**FIGURE 8.** Error index values on DDM (RE values).

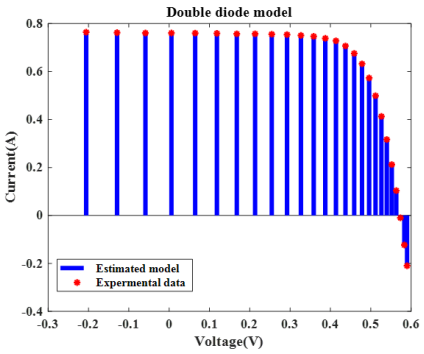


**FIGURE 9.** MFSMA for PV (I–V characteristics).

superiority is evident despite the subpar performance of other competing algorithms in these domains. Furthermore, MFSMA demonstrates supremacy in statistical significance when subjected to the Wilcoxon signed-rank test. Complementing this, Table 10 displays the confidence intervals for parameter estimation, calculated with a 95 percent certainty. It is within this stringent confidence threshold that MFSMA maintains the narrowest intervals of uncertainty for each parameter, underscoring its robustness as evidenced in Table 10. In summary, the MFSMA methodology proposed in this study proves to be adept at accurately interpreting the DDM model's intricacies, thereby facilitating precise estimations of performance.

### 3) PV MODULE

Within this section, the MFSMA is employed to tackle the challenge of parameter estimation for the Photo Watt-PWP 201 PV module example. Figures 9 and 10 demonstrate that, across the full voltage spectrum, the I-V and P-V characteristics derived from MFSMA closely mirror the authentic data as well as the simulated data, showcasing an exceptional fit with the experimental records. Moreover, Figures 12 and 11 display the error indices characterized by IAE and RE values. Notably, all IAE values are maintained below 5.088463e-3, while the bounds for RE are capped at 1.341222E-01 and -1.164536E-02, underscoring the precision of MFSMA in accurately capturing the true behaviors of PV module operations. Additionally, Table 11 consolidates the outcome of the IAE assessments regarding the PV mode, documenting a cumulative sum of these metrics at 0.065233288 and 0.753101573. Such metrics attest to the high-quality accuracy of the parameters obtained through the MFSMA. Consequently, the efficacy of MFSMA in

**TABLE 9.** RMSE of DDM.

| Algorithms | RMSE | | | | | |
|---|---|---|---|---|---|---|
| | Min | Median | Mean | Max | SD | Sig |
| NPSOPC | 7.65834E-04 | 8.521268E-04 | 9.320987E-04 | 9.688976E-04 | 3.254456E-04 | + |
| BLPSO | 1.015677E-03 | 1.105678E-03 | 1.151450E-03 | 1.521675E-03 | 1.657356E-04 | + |
| CLPSO | 1.023453E-03 | 1.093898E-03 | 1.122345E-03 | 1.402876E-03 | 5.442234E-04 | + |
| GOTLBO | 1.300980E-03 | 1.131457E-03 | 1.045456E-03 | 4.433567E-03 | 1.043435E-04 | + |
| EMSFLA | 9.723567E-04 | 9.781346E-04 | 9.328265E-04 | 9.689846E-04 | 1.432186E-06 | + |
| MLCPA | 8.521568E-04 | 8.854898E-04 | 7.652543E-04 | 9.452456E-04 | 1.251456E-06 | + |
| MFSMA | 7.689770E-04 | 7.656760E-04 | 6.789870E-04 | 8.767890E-04 | 8.987000E-07 | |

**TABLE 10.** Confidence intervals on DDM.

| Parameters | Algorithms | | | | | | |
|---|---|---|---|---|---|---|---|
| | NPSOPC | BLPSO | CLPSO | GOTLBO | EMSFLA | MLCPA | MFSMA |
| $I_{ph}$( A) | (0.631 0.786) | (0.676 0.793) | (0.481 0.764) | (0.698 0.773) | (0.749 0.757) | (0.751 0.758) | (0.752 0.756) |
| $I_{sd1}(\mu A)$ | (0.652 0.856) | (0.581 0.745) | (0.679 0.777) | (0.721 0.796) | (0.747 0.765) | (0.749 0.759) | (0.750 0.758) |
| $I_{sd2}(\mu A)$ | (0.124 0.345) | (0.138 0.322) | (0.143 0.243) | (0.178 0.245) | (0.216 0.237) | (0.217 0.238) | (0.216 0.234) |
| $R_S(\Omega)$ | (0.012 0.59) | (0.031 0.46) | (0.024 0.541) | (0.034 0.054) | (0.035 0.042) | (0.036 0.041) | (0.035 0.042) |
| $R_{\rm sh}(\Omega)$ | (38.79 56.43) | (38.79 55.46) | (48.47 57.55) | (49.53 58.53) | (55.43 55.58) | (55.45 55.59) | (55.46 55.60) |
| $n_1$ | (1.111 1.856) | (1.215 1.655) | (1.005 1.588) | (1.004 1.586) | (1.036 1.452) | (1.038 1.451) | (1.039 1.450) |
| $n_2$ | (1.019 1.639) | (1.029 1.554) | (1.329 1.923) | (1.032 1.626) | (1.201 1.389) | (1.213 1.383) | (1.216 1.380) |

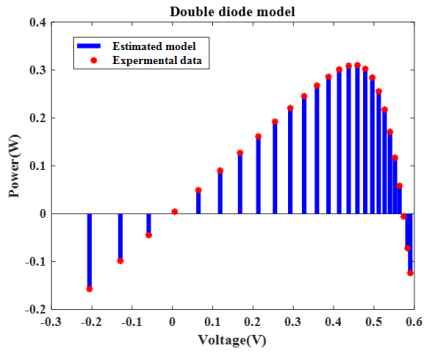


**FIGURE 10.** MFSMA for PV (P–V characteristics).

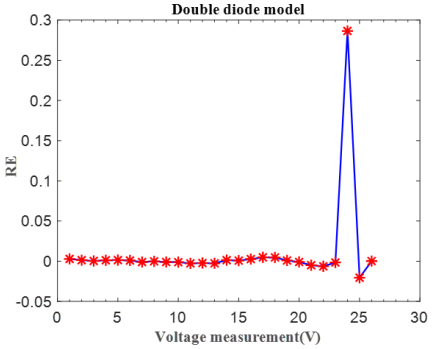


**FIGURE 12.** Error index values on PV (RE values).

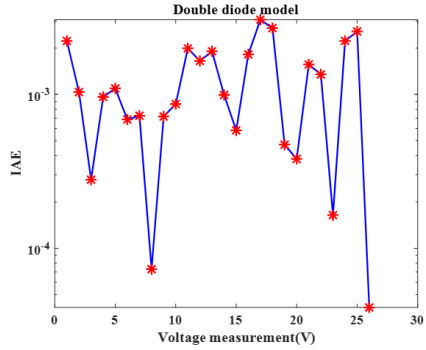


**FIGURE 11.** Error index values on PV (IAE values).

addressing this matter is consistently validated, reinforcing its stature as a robust tool for parameter estimation in PV modules.

Table 12 presents a comprehensive comparison of the MFSMA against a range of competing algorithms within the context of photovoltaic module optimization. The data clearly shows that the proposed MFSMA technique outclasses its competitors, achieving an average RMSE of 3.023098E-04 and an impressively low standard deviation of 1.232232E-06. While BLPSO and NPSOPC exhibit mean RMSEs that are somewhat comparable, EMSFLA takes second place in overall performance, edging out GOTLBO. When subjected to the Wilcoxon signed-rank test, MFSMA demonstrates significant superiority over alternate algorithms in this photovoltaic scenario. Furthermore, Table 13 details the confidence intervals for parameter estimations at a robust 95 percent confidence level. According to this table, the MFSMA consistently exhibits the least amount of dispersion across all parameters, validating its capability to precisely retrieve the characteristic parameters of the PV model. This proficiency is paralleled by the pattern observed in both SDM and DDM case studies, further confirming the algorithm's efficacy and reliability.

**TABLE 11.** IAE of MFSMA on PV module.

| Item | Measured data | | Simulated current data | | Simulated power data | |
|---|---|---|---|---|---|---|
| | V(V) | I(A) | Isim(A) | IAE1(A) | Psim(W) | IAEp(A) |
| 1 | 0.1248 | 1.0315 | 1.02974217 | 0.001757342 | 0.12851182 | 0.000223457 |
| 2 | 1.8093 | 1.03 | 1.02790803 | 0.002098908 | 1.859794 | 0.003897897 |
| 3 | 3.3511 | 1.026 | 1.02617315 | 0.000189079 | 3.43880885 | 0.000580346 |
| 4 | 4.7622 | 1.022 | 1.02443458 | 0.002433891 | 4.87856236 | 0.011678999 |
| 5 | 6.0538 | 1.018 | 1.02249303 | 0.004493033 | 6.18996832 | 0.027234568 |
| 6 | 7.2364 | 1.0155 | 1.01996408 | 0.004464082 | 7.38086808 | 0.032303457 |
| 7 | 8.3189 | 1.014 | 1.01616587 | 0.002156789 | 8.45338228 | 0.01801679 |
| 8 | 9.3097 | 1.01 | 1.00999155 | 8.41E-06 | 9.40271832 | 7.86769E-05 |
| 9 | 10.2163 | 1.0035 | 0.99974807 | 0.003890879 | 10.2137262 | 0.038345679 |
| 10 | 11.0449 | 0.988 | 0.98326771 | 0.004989099 | 10.8600936 | 0.052278988 |
| 11 | 11.8018 | 0.963 | 0.95790771 | 0.005089099 | 11.3050352 | 0.06008979 |
| 12 | 12.4929 | 0.9255 | 0.92107763 | 0.004423379 | 11.5069307 | 0.05678979 |
| 13 | 13.1231 | 0.8725 | 0.87097927 | 0.001520389 | 11.4299481 | 0.019921212 |
| 14 | 13.6983 | 0.8075 | 0.80616172 | 0.001338282 | 11.0430451 | 0.018434343 |
| 15 | 14.2221 | 0.7265 | 0.72801642 | 0.001789895 | 10.3539224 | 0.021565657 |
| 16 | 14.6995 | 0.6345 | 0.63779343 | 0.003346759 | 9.37524455 | 0.048411734 |
| 17 | 15.1346 | 0.5345 | 0.53786212 | 0.003378999 | 8.14032805 | 0.050885668 |
| 18 | 15.5311 | 0.4275 | 0.431932 | 0.004448489 | 6.70837909 | 0.068838935 |
| 19 | 15.8929 | 0.3185 | 0.32165994 | 0.003132323 | 5.11210933 | 0.050223445 |
| 20 | 16.2229 | 0.2085 | 0.21027785 | 0.001767899 | 3.41131648 | 0.026732123 |
| 21 | 16.5241 | 0.101 | 0.09862038 | 0.002378765 | 1.62961304 | 0.038978654 |
| 22 | 16.7987 | -0.008 | -0.0070547 | 0.000945679 | -0.11850928 | 0.01589879 |
| 23 | 17.0499 | -0.111 | -0.1112143 | 0.000214256 | -1.89619194 | 0.003667893 |
| 24 | 17.2793 | -0.209 | -0.2114803 | 0.002483329 | -3.6542324 | 0.043456789 |
| 25 | 17.4885 | -0.303 | -0.3054941 | 0.002494233 | -5.34263409 | 0.044567892 |
| Sun of IAE | / | / | / | 0.065233288 | / | 0.753101573 |

**TABLE 12.** RMSE values of PV.

| Algorithm | RMSE | | | | | |
|---|---|---|---|---|---|---|
| | Min | Median | Mean | Max | SD | Sig |
| NPSOPC | 1.235654E-03 | 1.563321E-03 | 2.415789E-03 | 2.684655E-03 | 2.421543E-04 | + |
| BLPSO | 1.203655E-03 | 1.634453E-03 | 1.482675E-03 | 2.205567E-03 | 2.337765E-04 | + |
| CLPSO | 1.205435E-03 | 1.214435E-03 | 1.131898E-03 | 2.313456E-03 | 3.457344E-04 | + |
| GOTLBO | 1.5014325E-03 | 1.313456E-03 | 1.213543E-03 | 2.214423E-03 | 2.454324E-04 | + |
| EMSFLA | 6.301510E-04 | 5.352678E-04 | 6.536789E-04 | 7.879878E-04 | 1.637896E-06 | + |
| MLCPA | 4.212345E-04 | 4.352345E-04 | 5.125675E-04 | 6.522345E-04 | 1.426546E-06 | + |
| MFSMA | 3.111098E-04 | 3.352230E-04 | 3.023098E-04 | 2.221897E-04 | 1.232232E-06 | |

**TABLE 13.** Confidence intervals on PV.

| Parameters | Algorithm | | | | | | |
|---|---|---|---|---|---|---|---|
| | NPSOPC | BLPSO | CLPSO | GOTLBO | EMSFLA | MLCPA | MFSMA |
| $I_{ph}$( A) | (0.584 0.765) | (0.668 0.788) | (0.585 0.764) | (0.688 0.783) | (0.768 0.779) | (0.770 0.779) | (0.772 0.775) |
| $I_{sd1}(\mu A)$ | (0.451 0.778) | (0.590 0.754) | (0.656 0.768) | (0.721 0.834) | (0.728 0.763) | (0.727 0.756) | (0.729 0.750) |
| $I_{sd2}(\mu A)$ | (0.112 0.454) | (0.126 0.338) | (0.123 0.255) | (0.198 0.258) | (0.211 0.244) | (0.204 0.228) | (0.214 0.220) |
| $R_s(\Omega)$ | (0.046 0.623) | (0.034 0.38) | (0.024 0.66) | (0.028 0.054) | (0.038 0.049) | (0.027 0.036) | (0.028 0.033) |
| $R_{sh}(\Omega)$ | (40.26 55.46) | (38.84 54.38) | (48.57 57.68) | (49.47 58.48) | (55.43 55.58) | (55.34 55.49) | (55.36 55.47) |
| $n_1$ | (1.103 1.842) | (1.188 1.578) | (1.012 1.684) | (1.089 1.656) | (1.024 1.363) | (1.018 1.258) | (1.019 1.248) |
| $n_2$ | (1.035 1.646) | (1.033 1.642) | (1.324 1.835 | (1.027 1.638) | (1.245 1.447) | (1.127 1.368) | (1.129 1.356) |

### C. RESULTS OF THE MANUFACTURER'S DATASHEET

In this study, we explore the validity of the proposed Maximum PowerPoint Tracking technique known as MFSMA through the analysis of a manufacturer's dataset. The dataset in question is comprised of multi-crystalline (KC200GT) photovoltaic samples, which have been gathered under a variety of temperature and irradiance conditions. By examining the ability of solar devices to recognize parameters across different temperatures or pressures, the robustness and adaptability of the MFSMA algorithm within complex

**TABLE 14. Optimal parameters with various irradiance under 25 °C on KC200GT.**

| Parameters | Irradiance | | | | |
|---|---|---|---|---|---|
| | 200 W/m$^2$ | 400 W/m$^2$ | 600 W/m$^2$ | 800 W/m$^2$ | 1000 W/m$^2$ |
| SDM | | | | | |
| $I_{Ph}$( A) | 1.646154479 | 3.28784893 | 4.934307945 | 6.571327377 | 8.216891461 |
| $I_{sd}(\mu A)$ | 5.20997E-10 | 1.48987E-09 | 3.86144E-09 | 9.53063E-10 | 2.24195E-09 |
| $R_s(\Omega)$ | 0.381111453 | 0.35357862 | 0.33733826 | 0.357335312 | 0.343814047 |
| $R_{\mathrm{sh}(\Omega)}$ | 690.1466111 | 752.0893857 | 743.0015919 | 743.523157 | 763.5351733 |
| $n$ | 1.003243464 | 1.05503875 | 1.104020542 | 1.035319708 | 1.076410285 |
| RMSE | 0.001418466 | 0.0014262 | 0.001297668 | 0.00163097 | 0.001539031 |
| DDM | | | | | |
| $I_{Ph}$( A) | 1.645937346 | 3.287848931 | 4.934307944 | 6.570513347 | 8.21684217 |
| $I_{sd1}(\mu A)$ | 4.84562E-10 | 1.48987E-09 | 1.51823E-17 | 5.52985E-08 | 2.19172E-06 |
| $I_{sd2}(\mu A)$ | 1.53073E-05 | 1.12133E-18 | 3.86144E-09 | 5.03735E-10 | 2.23103E-09 |
| $R_S(\Omega)$ | 0.383131626 | 0.353578609 | 0.33733826 | 0.361106414 | 0.343861097 |
| $R_{sh}(\Omega)$ | 709.501561 | 752.089397 | 743.0016353 | 800.6518791 | 767.6196281 |
| $n_1$ | 1 | 1.05503876 | 3.900635458 | 1.525357331 | 3.999999999 |
| $n_2$ | 4 | 3.999398783 | 1.104020542 | 1.008760998 | 1.076176379 |
| RMSE | 0.001409086 | 0.0014262 | 0.001297668 | 0.001504603 | 0.001538902 |

environments can be effectively assessed. Optimal parameters for both the single diode model (SDM) and double diode model (DDM) of two solar modules were identified through meticulous experimentation and statistical scrutiny at distinct irradiance levels while maintaining a constant temperature of 25°C. These findings are detailed in Tables 14. To corroborate the precision of the photovoltaic parameters obtained, the corresponding electrical current values were also evaluated.

The I-V characteristics of the two solar modules were charted across a spectrum of irradiance intensities—namely 200 W/m$^2$, 400 W/m$^2$, 600 W/m$^2$, 800 W/m$^2$, and 1000 W/m$^2$—as presented in Tables 15. For the SDM, the determined optimal parameters showed remarkable concurrence with the experimental data collected under varying conditions of temperature and irradiance. This attests to the capacity of MFSMA to maintain an acceptable RMSE value for the KC200GT in the context of SDM. Similarly, with the DDM, the conformity of the estimated results with the empirical datasets was evident, even under less-than-ideal environmental conditions characterized by extreme irradiance or temperature variations. In such challenging scenarios, the MFSMA algorithm continued to demonstrate its reliability by ensuring satisfactory RMSE values. Based on the foregoing evidence, it is reasonable to assert that the proposed MFSMA stands as a high-caliber method for the discernment of parameters in solar cell modules, prevailing even against the rigors of adverse conditions, such as high pressure or frigid temperatures. Consequently, the resilience of the MFSMA approach has been convincingly validated.

**TABLE 15. Optimal parameters with various temperatures under 1000 irradiance on KC200GT.**

| Parameters | Temperature | | |
|---|---|---|---|
| | 25°C | 50°C | 75°C |
| SDM | | | |
| $I_{Ph}$( A) | 8.208783231 | 8.27809373 | 8.36987393 |
| $I_{sd}(\mu A)$ | 2.134920E-09 | 1.246789E-07 | 1.789302E-06 |
| $R_s(\Omega)$ | 0.3478922 | 0.32098932 | 0.312380131 |
| $R_{sh}(\Omega)$ | 763.523938 | 953.378923 | 789.547323 |
| $n$ | 1.08978342 | 1.1129022 | 1.11293834 |
| RMSE | 0.001549383 | 0.00267892 | 0.00349403 |
| DDM | | | |
| $I_{Ph}$( A) | 8.2198982 | 8.28978934 | 8.3897882 |
| $I_{sd1}(\mu A)$ | 2.1892831E-06 | 1.789231E-07 | 1.789862E-06 |
| $I_{sd2}(\mu A)$ | 2.2103E-09 | 6.45023E-19 | 1.81283E-16 |
| $R_S(\Omega)$ | 0.3467891 | 0.3898223 | 0.33789873 |
| $R_{sh}(\Omega)$ | 767.6378928 | 953.898782 | 790.674892 |
| $n_1$ | 3.898278292 | 1.1010283 | 1.19882923 |
| $n_2$ | 1.078932 | 2.347898273 | 3.44789283 |
| RMSE | 0.001534889 | 0.002678934 | 0.004389242 |

## V. DISCUSSION

Extensive testing on the F1-F23 benchmark functions demonstrates a significant enhancement in the capabilities of MFSMA, thanks to the integration of new techniques. The method's effectiveness is further corroborated through an exhaustive analysis of photovoltaic performance parameter estimation using SDM, DDM, and PV modules based on data from a manufacturer's datasheet. Consequently, the proposed MFSMA algorithm emerges as a formidable contender among other competing algorithms for addressing the problem at hand. As detailed in section 3, the MFSMA underwent rigorous testing and comparison with several well-established algorithms across a range of unimodal, multimodal, and fixed-dimension multimodal benchmarks. In these comparisons, MFSMA not only consistently surpassed the original SMA but also demonstrated properties

that were markedly improved over its peers. Moreover, MFSMA was applied to parameter identification within three related solar module models. It is noteworthy that MFSMA accurately ascertained essential parameters for these models, showing high congruence with experimental recordings across the entire voltage spectrum. This precision indicates that MFSMA possesses a unique ability for exploitation that other algorithms may lack, giving it a distinct advantage in solving such problems. In summary, the key characteristics of MFSMA have undergone substantial refinements, as evidenced by various empirical datasets. These advancements position the MFSMA as a superior technique both in theory and application, capable of yielding reliable and precise outcomes in the field of photovoltaic parameter estimation.

The MFSMA's robustness and efficacy were further assessed using data from a manufacturer, specifically under extreme conditions such as high pressure or low temperatures. As a result, the MFSMA may be considered a viable approach for characterizing solar cells that exhibit consistent long-term stability in performance. The proposed MFSMA is not solely applicable to the case studies within this research; it has potential utility in other domains, including power engineering. Looking ahead, the MFSMA could be employed to determine optimal settings for a variety of complex challenges. Additionally, it is important to acknowledge the limitations inherent to the algorithm proposed in this paper. Firstly, while this paper introduces new operators to enhance the original SMA, there is an associated increase in computational time. This trade-off implies that efficiency is somewhat compromised in favor of improved performance. Secondly, the algorithm was designed with a focus on single-objective optimization, which might not suffice for applications requiring robust multi-objective algorithms. Lastly, the dataset utilized in this study, although open source, is quite limited. For a more comprehensive evaluation of the algorithm's performance, it would be ideal to test it against data drawn from real-world scenarios.

## VI. CONCLUSION AND FUTURE WORK

In this paper, multi-strategy learning fusion Slime Mould Algorithm to extract the solar cell model parameters and photovoltaic modules. Based on the above experimental results, some conclusions can be drawn as follows:

- Benchmark results demonstrate that the inherent capabilities of the conventional Slime Mould Algorithm (SMA) can be augmented by leveraging the distinctive mechanisms of opposition-based learning. Furthermore, the integration of level-based learning contributes to a more consistent equilibrium between intensification and diversification strategies.
- The outcomes of the investigations indicate that MFSMA possesses a discernible superiority over its competitors in estimating diverse parameters of photovoltaic systems.
- The MFSMA exhibits robust performance under extreme conditions, maintaining its functionality both under high-pressure scenarios and in frigid temperatures.

Considering the noticeable gap in the numerical evaluation concerning the efficiency and computational time trade-off, future research directions should emphasize exploring parallel computing or GPU-based algorithms. This approach aims to thoroughly assess how leveraging parallel processing or GPUs can mediate the balance between achieving high computational efficiency and minimizing execution time. By focusing on these technologies, researchers could develop innovative strategies that exploit the parallelism inherent in GPUs or distributed computing environments to optimize both efficiency and speed.

## ACKNOWLEDGMENT

The authors extend their deepest gratitude to the Editor-in-Chief, Associate Editors, and the anonymous reviewers for their diligent efforts in reviewing their manuscript. Their insightful comments and suggestions have been invaluable in enhancing the quality of their work.

## REFERENCES

[1] F. Belaïd, A. Al-Sarihi, and R. Al-Mestneer, "Balancing climate mitigation and energy security goals amid converging global energy crises: The role of green investments," *Renew. Energy*, vol. 205, pp. 534–542, Mar. 2023.

[2] G. S. Steele, "Confronting the 'climate lehman moment': The case for macroprudential climate regulation," *Cornell JL Pub. Pol'y*, vol. 30, p. 109, Jun. 2020.

[3] L. H. Melnyk, L. V. Shaulska, O. I. Matsenko, V. S. Piven, and V. V. Konoplov, "Modern trends in the production of renewable energy: The cost benefit approach," *Mechanism Econ. Regulation*, vol. 91, no. 1, pp. 6–17, 2021.

[4] J. Li, S. Chen, Y. Wu, Q. Wang, X. Liu, L. Qi, X. Lu, and L. Gao, "How to make better use of intermittent and variable energy? A review of wind and photovoltaic power consumption in China," *Renew. Sustain. Energy Rev.*, vol. 137, Mar. 2021, Art. no. 110626.

[5] E. Bullich-Massagué, F.-J. Cifuentes-García, I. Glenny-Crende, M. Cheah-Mañé, M. Aragüés-Peñalba, F. Díaz-González, and O. Gomis-Bellmunt, "A review of energy storage technologies for large scale photovoltaic power plants," *Appl. Energy*, vol. 274, Sep. 2020, Art. no. 115213.

[6] Y. Feng, W. Hao, H. Li, N. Cui, D. Gong, and L. Gao, "Machine learning models to quantify and map daily global solar radiation and photovoltaic power," *Renew. Sustain. Energy Rev.*, vol. 118, Feb. 2020, Art. no. 109393.

[7] M. J. Mayer and G. Gróf, "Extensive comparison of physical models for photovoltaic power forecasting," *Appl. Energy*, vol. 283, Feb. 2021, Art. no. 116239.

[8] A. Mellit, A. M. Pavan, and V. Lughi, "Deep learning neural networks for short-term photovoltaic power forecasting," *Renew. Energy*, vol. 172, pp. 276–288, Jul. 2021.

[9] S. Li, H. Chen, M. Wang, A. A. Heidari, and S. Mirjalili, "Slime mould algorithm: A new method for stochastic optimization," *Future Gener. Comput. Syst.*, vol. 111, pp. 300–323, Oct. 2020.

[10] C. Li, J. Li, H. Chen, M. Jin, and H. Ren, "Enhanced Harris hawks optimization with multi-strategy for global optimization tasks," *Exp. Syst. Appl.*, vol. 185, Dec. 2021, Art. no. 115499.

[11] Y. Yang, H. Chen, A. A. Heidari, and A. H. Gandomi, "Hunger games search: Visions, conception, implementation, deep analysis, perspectives, and towards performance shifts," *Expert Syst. Appl.*, vol. 177, Sep. 2021, Art. no. 114864.

[12] H. Shaban, E. H. Houssein, M. Pérez-Cisneros, D. Oliva, A. Y. Hassan, A. A. K. Ismaeel, D. S. AbdElminaam, S. Deb, and M. Said, "Identification of parameters in photovoltaic models through a Runge Kutta optimizer," *Mathematics*, vol. 9, no. 18, p. 2313, Sep. 2021.

[13] J. Tu, H. Chen, M. Wang, and A. H. Gandomi, "The colony predation algorithm," *J. Bionic Eng.*, vol. 18, no. 3, pp. 674–710, May 2021.
[14] I. Ahmadianfar, A. A. Heidari, S. Noshadian, H. Chen, and A. H. Gandomi, "INFO: An efficient optimization algorithm based on weighted mean of vectors," *Exp. Syst. Appl.*, vol. 195, Jun. 2022, Art. no. 116516.
[15] S. Mirjalili, S. M. Mirjalili, and A. Lewis, "Grey wolf optimizer," *Adv. Eng. Softw.*, vol. 69, pp. 46–61, Mar. 2014.
[16] Y. Song, D. Wu, W. Deng, X.-Z. Gao, T. Li, B. Zhang, and Y. Li, "MPPCEDE: Multi-population parallel co-evolutionary differential evolution for parameter optimization," *Energy Convers. Manage.*, vol. 228, Jan. 2021, Art. no. 113661.
[17] X. Chen, H. Yue, and K. Yu, "Perturbed stochastic fractal search for solar PV parameter estimation," *Energy*, vol. 189, Dec. 2019, Art. no. 116247.
[18] D. Yousri, S. B. Thanikanti, D. Allam, V. K. Ramachandaramurthy, and M. B. Eteiba, "Fractional chaotic ensemble particle swarm optimizer for identifying the single, double, and three diode photovoltaic models' parameters," *Energy*, vol. 195, Mar. 2020, Art. no. 116979.
[19] N. Lynn and P. N. Suganthan, "Ensemble particle swarm optimizer," *Appl. Soft Comput.*, vol. 55, pp. 533–548, Jun. 2017.
[20] F. Dkhichi, B. Oukarfi, A. Fakkar, and N. Belbounaguia, "Parameter identification of solar cell model using Levenberg–Marquardt algorithm combined with simulated annealing," *Sol. Energy*, vol. 110, pp. 781–788, Dec. 2014.
[21] S. Kirkpatrick, C. D. Gelatt Jr., and M. P. Vecchi, "Optimization by simulated annealing," *Science*, vol. 220, no. 4598, pp. 671–680, 4598.
[22] B. Li, H. Wang, X. Wang, M. Negnevitsky, and C. Li, "Tri-stage optimal scheduling for an islanded microgrid based on a quantum adaptive sparrow search algorithm," *Energy Convers. Manage.*, vol. 261, Jun. 2022, Art. no. 115639.
[23] R. Abbassi, A. Abbassi, A. A. Heidari, and S. Mirjalili, "An efficient salp swarm-inspired algorithm for parameters identification of photovoltaic cell models," *Energy Convers. Manage.*, vol. 179, pp. 362–372, Jan. 2019.
[24] S. Mirjalili, A. H. Gandomi, S. Z. Mirjalili, S. Saremi, H. Faris, and S. M. Mirjalili, "Salp swarm algorithm: A bio-inspired optimizer for engineering design problems," *Adv. Eng. Softw.*, vol. 114, pp. 163–191, Dec. 2017.
[25] D. H. Wolpert and W. G. Macready, "No free lunch theorems for optimization," *IEEE Trans. Evol. Comput.*, vol. 1, no. 1, pp. 67–82, Apr. 1997.
[26] H. R. Tizhoosh and M. Ventresca, *Oppositional Concepts in Computational Intelligence*, vol. 155. Springer, 2008.
[27] S. Mahdavi, S. Rahnamayan, and K. Deb, "Opposition based learning: A literature review," *Swarm Evol. Comput.*, vol. 39, pp. 1–23, Apr. 2018.
[28] W. Deng, H. Ni, Y. Liu, H. Chen, and H. Zhao, "An adaptive differential evolution algorithm based on belief space and generalized opposition-based learning for resource allocation," *Appl. Soft Comput.*, vol. 127, Sep. 2022, Art. no. 109419.
[29] B. S. Yildiz, N. Pholdee, S. Bureerat, A. R. Yildiz, and S. M. Sait, "Enhanced grasshopper optimization algorithm using elite opposition-based learning for solving real-world engineering problems," *Eng. Comput.*, vol. 38, no. 5, pp. 4207–4219, Oct. 2022.
[30] H. Chen, A. A. Heidari, H. Chen, M. Wang, Z. Pan, and A. H. Gandomi, "Multi-population differential evolution-assisted Harris hawks optimization: Framework and case studies," *Future Gener. Comput. Syst.*, vol. 111, pp. 175–198, Oct. 2020.
[31] A. Alihodzic and M. Tuba, "Bat algorithm (Ba) for image thresholding," in *Proc. 12th Int. Conf. Signal Process. (SIP)*. Baltimore, MD, USA: Morgan State Univ., 2013, pp. 17–19.
[32] F. Marini and B. Walczak, "Particle swarm optimization (PSO). A tutorial," *Chemometric Intell. Lab. Syst.*, vol. 149, pp. 153–165, Dec. 2015.
[33] I. Fister, I. Fister, X.-S. Yang, and J. Brest, "A comprehensive review of firefly algorithms," *Swarm Evol. Comput.*, vol. 13, pp. 34–46, Dec. 2013.
[34] E. Rashedi, H. Nezamabadi-pour, and S. Saryazdi, "GSA: A gravitational search algorithm," *Inf. Sci.*, vol. 179, no. 13, pp. 2232–2248, Jun. 2009.
[35] X. Lin and Y. Wu, "Parameters identification of photovoltaic models using niche-based particle swarm optimization in parallel computing architecture," *Energy*, vol. 196, Apr. 2020, Art. no. 117054.
[36] J. Liang, S. Ge, B. Qu, K. Yu, F. Liu, H. Yang, P. Wei, and Z. Li, "Classified perturbation mutation based particle swarm optimization algorithm for parameters extraction of photovoltaic models," *Energy Convers. Manage.*, vol. 203, Jan. 2020, Art. no. 112138.
[37] X. Chen, K. Yu, W. Du, W. Zhao, and G. Liu, "Parameters identification of solar cell models using generalized oppositional teaching learning based optimization," *Energy*, vol. 99, pp. 170–180, Mar. 2016.
[38] M. Wang, Q. Zhang, H. Chen, A. A. Heidari, M. Mafarja, and H. Turabieh, "Evaluation of constraint in photovoltaic cells using ensemble multi-strategy shuffled frog leading algorithms," *Energy Convers. Manage.*, vol. 244, Sep. 2021, Art. no. 114484.

**CHI CHEN** is currently an Associate Professor with Wenzhou University of Technology. He has once served as the Deputy Director (temporary) of the Data Resources Division of Wenzhou Big Data Development Administration and a Senior Technical Manager with China Telecom Wenzhou Branch. Obtained the title of China Telecom Group-Level Talent, Zhejiang Province Telecom first-level Expert, and Oracle OCM certified expert. He has published many SCI articles and has rich practical experience in database design and optimization, software development, big data architecture, and data mining.

**XIAN CHEN** is currently a Teacher with Wenzhou Polytechnic, Wenzhou, Zhejiang, China, engaged in research directions, such as data mining and intelligent computing.

**AIJU LIN** is currently a Professor with specializing in Wenzhou University. She teaches courses on career development and employment guidance for university students. She has been honored with several accolades, including the Third Prize for Applied Achievements in Philosophy and Social Sciences at the 16th Wenzhou City Awards, in 2017. She is also recognized as an Outstanding Mentor with the Ninth Zhejiang Province University Students' Career Planning and Entrepreneurship Competition and has guided her team to win the Silver Award for Public Welfare Entrepreneurship in the "Challenge Cup" National College Student Entrepreneurship Contest.